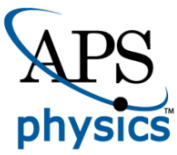

Observation of Rapid Adiabatic Passage in Optical Four-Wave Mixing

Xiaoyue Ding, Dylan Heberle, Kerrianne Harrington, Noah Flemens, Wei-Zung Chang, Tim A. Birks, and Jeffrey Moses

Phys. Rev. Lett. **124**, 153902 — Published 14 April 2020

DOI: 10.1103/PhysRevLett.124.153902

Observation of rapid adiabatic passage in optical four-wave mixing

Xiaoyue Ding,[1] Dylan Heberle,[1] Kerrianne Harrington,[2] Noah Flemens,[1] Wei-Zung Chang,[1] Tim A. Birks,[2] and Jeffrey Moses[1,*]

[1]*School of Applied and Engineering Physics, Cornell University, Ithaca, NY 14853, USA*
[2]*Department of Physics, University of Bath, Claverton Down, Bath BA2 7AY, UK*

(Dated: February 18, 2020)

We observe clear evidence of adiabatic passage between photon populations via a four-wave mixing process, implemented through a dispersion sweep arranged by a core diameter taper of an optical fiber. Photonic rapid adiabatic passage through the cubic electric susceptibility thus opens precise control of frequency translation between broadband light fields to all common optical media. Areas of potential impact include optical fiber and on-chip waveguide platforms for quantum information, ultrafast spectroscopy and metrology, and extreme light-matter interaction science.

When two classical or quantum light waves of disparate frequencies are coupled in a nonlinear optical medium in the presence of one or more classical pump waves, their evolution equations take the form of a coupled quantum two-state system [1, 2]. Recent advances in photonics-based quantum information processing have made use of the analogy, including wavelength-domain Hadamard operations and Ramsey interference on single photons as well as wavelength-domain HongOuMandel interference between photon pairs [3–7].

However, the physics of optical frequency conversion shares a fundamental problem with the control of populations in inhomogeneous quantum two-state systems. In broadband frequency conversion, the varying momentum mismatch (known as the wave-vector mismatch) over the range of frequencies involved creates an ensemble inhomogeneity. As a result, efficient conversion is limited to only a narrow bandwidth near a perfectly wave-vector matched frequency, and a broader conversion bandwidth can only be achieved by sacrificing efficiency, known as the bandwidth-efficiency trade-off. The same problems occur in quantum two-level systems with an ensemble inhomogeneity: a non-uniform resonance frequency limits a complete population inversion or any alternative desired quantum state preparation to a fraction of the ensemble. A solution for the latter platform has long been established: rapid adiabatic passage (RAP) produces a robust population inversion in nuclear magnetic resonance and in atoms or molecules without need for electromagnetic coupling pulses of a precise integrated power and overcomes the impurity in quantum state preparation from inhomogeneous ensembles [8–11].

Thus motivated, the concept of RAP in a parametric three-wave mixing (TWM) frequency down- or up-conversion process was proposed in analogy to RAP in quantum two-level systems a decade ago [12]. It was since demonstrated in spectacular fashion using a slow sweep of the wave-vector mismatch through a quadratic electric susceptibility ($\chi^{(2)}$) poled aperiodically and longitudinally. Adiabatic inversion of the photon population of an octave-spanning pulse was achieved with an efficiency above 90% and with close adherence to the theoretical Landau-Zener (LZ) adiabatic transition efficiency [13, 14]. Taking advantage of a linearized phase and amplitude transfer between photon populations, arbitrary shaping of octave-spanning mid-infrared pulses was achieved, with potential applications to time-resolved spectroscopy and phase-controlled strong-field interactions at the single-cycle duration extreme [15]. The method could also be beneficial to the processing of broadband nonclassical light fields. These implementations were carried out using specialized noncentrosymmetric ferroelectric crystals with $\chi^{(2)}$ poling. To allow the RAP concept to be applied universally, it must be achievable through the cubic nonlinear susceptibility ($\chi^{(3)}$), which is present in all materials and thus relevant to all optical platforms. RAP in optical four-wave mixing (FWM) in cubic nonlinear media was recently predicted with several key differences to adiabatic TWM [16]: the effects of self-phase modulation (SPM) and cross-phase modulation (XPM) always accompany FWM and represent potentially competing effects in the wave evolution, and as poling of $\chi^{(3)}$ has not been achieved, the use of aperiodic quasi-phase matching to achieve a longitudinal variation of the wave-vector mismatch must be replaced by another means.

In this Letter, we demonstrate clear evidence of RAP between photon populations mediated by $\chi^{(3)}$ in an optical fiber. Adiabatic FWM (AFWM) is demonstrated through frequency down-conversion by Bragg-scattering (BS) FWM in a simple photonic crystal fiber (PCF) with a core taper that allows the wave-vector mismatch to be adiabatically swept during propagation. We observe adherence of the field-amplitude frequency conversion to the LZ efficiency of RAP, which has the character of a near-unitary photon number population inversion for the classical signal field used in this demonstration. We also observe the spectral domain signature of RAP: a conversion band evolution that is no longer subject to a wave-vector-matching acceptance bandwidth, resulting in an order-of-magnitude larger conversion bandwidth compared to an ordinary BS FWM process with uniform and close-to-

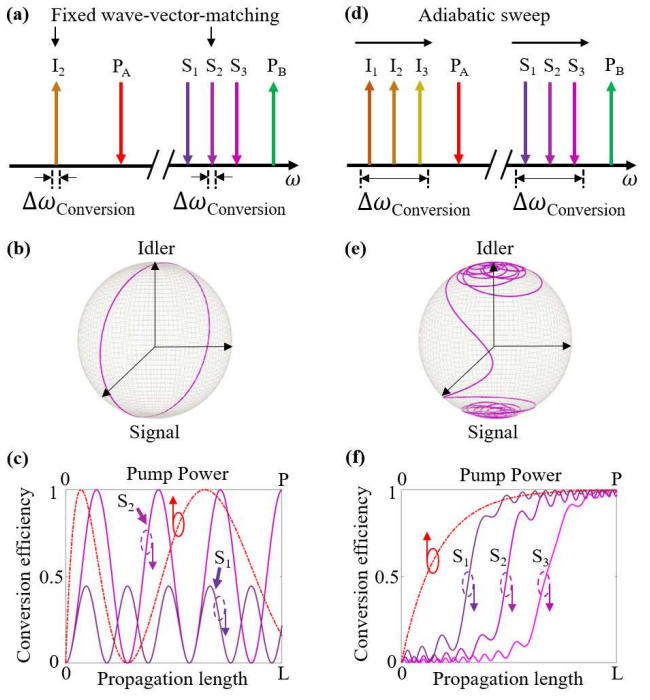

FIG. 1. BS FWM with fixed (a-c) vs. adiabatically sweeping (d-f) wave-vector-matching $\Delta k_{\rm eff}$ condition. $\rm P_A$, $\rm P_B$: non-degenerate pump photons. $\rm S_i$ $(i = 1, 2, 3)$: signal photons. $\rm I_i$ $(i = 1, 2, 3)$: idler photons. Whereas (a) fixed $\Delta k_{\rm eff}$ selects a limited conversion band $\rm S_2 \leftrightarrow I_2$, (d) adiabatic conversion sequentially converts much wider bandwidth $\rm S_i \leftrightarrow I_i$ $(i = 1, 2, 3)$. Bloch sphere representations show (b) Rabi flopping vs. (e) adiabatic following dynamics. (c) Oscillatory, frequency-selective power- and length-dependent conversion dynamics of constant $\Delta k_{\rm eff}$ contrast with (f) saturating, uniform conversion dynamics of the adiabatic case.

unity conversion. Moreover, we find AFWM to be robust to observed coexisting XPM. Open to platforms suitable for low intensity fields such as the highly nonlinear fiber platform used here and potentially on-chip silicon waveguides [16], AFWM might be used for the processing of photonic qubits over wide bandwidths. Also open to high-flux platforms such as gas-filled fibers, AFWM might be used for the control of strong-field and attosecond domain light-matter interactions [17–22], the spectroscopy of ultrafast photo-induced molecular dynamics [23], laser-based particle acceleration [24], all-optical signal processing [25, 26], and up-conversion imaging [27].

A BS FWM process involves four distinct optical fields that exchange photon populations (Fig. 1(a)), two pumps, a signal, and an idler. Annihilation of a pump photon A and a signal photon accompanies creation of a pump photon B and an idler photon such that $\omega_{\rm A} + \omega_{\rm Sig} = \omega_{\rm B} + \omega_{\rm Idl}$. For sufficiently strong pump fields, the signal and idler obey coupled equations analogous to the two-state time-dependent Schrdinger equation [16],

$$\frac{d}{dz}\begin{bmatrix} C_{\rm Sig} \\ C_{\rm Idl} \end{bmatrix} = \frac{i}{2}\begin{bmatrix} \Delta k_{\rm eff} & \kappa \\ \kappa & -\Delta k_{\rm eff} \end{bmatrix}\begin{bmatrix} C_{\rm Sig} \\ C_{\rm Idl} \end{bmatrix}, \quad (1)$$

where z is the propagation distance and $\rm C_{Sig}$ and $\rm C_{Idl}$ are normalized field amplitudes of the signal and idler, respectively. $\Delta k_{\rm eff} = \Delta k + \Delta k_{\rm PM}$ is the effective wave-vector mismatch, with $\Delta k = k_{\rm Sig} - k_{\rm Idl} + k_{\rm A} - k_{\rm B}$ equal to the wave-vector mismatch of the four waves (playing the role of frequency detuning in the quantum two-level model) and $\Delta k_{\rm PM}$ equal to a shift due to SPM and XPM (analogous to a Stark-induced transition energy shift). $\kappa = 2\gamma\sqrt{P_{\rm A} P_{\rm B}}$ is the nonlinear coupling strength (equivalent to a Rabi frequency), with γ a $\chi^{(3)}$-dependent characteristic nonlinear coefficient and $P_i, (i = \rm A,B)$ the power of the two pump waves. A characteristic nonlinear length can be defined as $L_{NL} = 1/\kappa$ (equivalent to a Rabi oscillation period). Under the condition of $\Delta k_{\rm eff} = 0$, known as perfect phase matching (analogous to resonance), the signal/idler photon state vector evolution traces a great-circle arc on the surface of a Bloch sphere, Fig. 1(b), where the south/north poles represent pure signal/idler states. The vector rotation produces BS FWM frequency conversion and back-conversion cycles analogous to resonant Rabi oscillations, with the conversion efficiency strongly dependent on pump power for a given nonlinear medium length (Fig. 1(c)). High-efficiency conversion is tightly restricted to frequencies near the perfectly phase-matched frequency, as all other frequencies have $|\Delta k_{\rm eff}| > 0$, resulting in rapid low-efficiency conversion cycles (analogous to detuned Rabi flopping). AFWM overcomes this limitation by adiabatically sweeping $\Delta k_{\rm eff}$ from large negative (positive) value to large positive (negative) value, resulting in RAP. Assuming the system starts in a pure signal state, if the sweeping rate fulfills the adiabatic condition,

$$|\dot{\kappa}\Delta k_{\rm eff} - \kappa\Delta\dot{k}_{\rm eff}| \ll (\kappa^2 + \Delta k_{\rm eff}^2)^{\frac{3}{2}} \quad (2)$$

(where derivatives are with respect to z), the signal/idler photon state vector undergoes a spiral trace on the surface of the Bloch sphere, creating a complete photon population inversion (Fig. 1(e)). The resulting idler generation is not only back-conversion-free, but can also cover orders-of-magnitude larger bandwidth since the sweeping dispersion can traverse the phase-matching condition $(\Delta k_{\rm eff} = 0)$ for all present frequencies (Fig. 1(d,f)). For a constant sweep rate, the population inversion efficiency of RAP was described by Landau and Zener [8, 9], which, in the context of AFWM is

$$\eta_{LZ} = 1 - \exp(-8\pi\kappa^2/(\partial\Delta k_{\rm eff}/\partial z)). \quad (3)$$

Eq. 3 describes an efficiency that saturates exponentially with increasing coupling strength κ, thus asymptotically reaching 100% at high pump powers (Fig. 1(f)). $L_{ad} = 1/\kappa^2$ is a characteristic adiabatic conversion length.

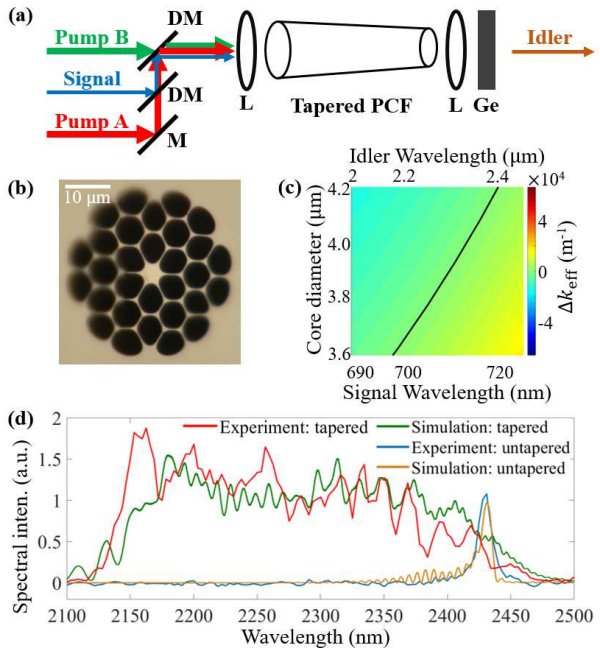

FIG. 2. (a) Experimental implementation of AFWM. M: high reflectivity mirror; DM: dichroic mirror; L: lens. Ge: Germanium window. (b) Optical microscope image of the PCF cross-section. (c) Map of Δk_{eff} vs. fiber core diameter and signal/idler wavelength pairs, with $\Delta k_{\text{eff}} = 0$ indicated in black. Calculations were performed by finite-element analysis of the fundamental mode propagation constants. (d) Measured experimental compared to simulated idler spectra for tapered (AFWM) and untapered (regular BS FWM) PCF.

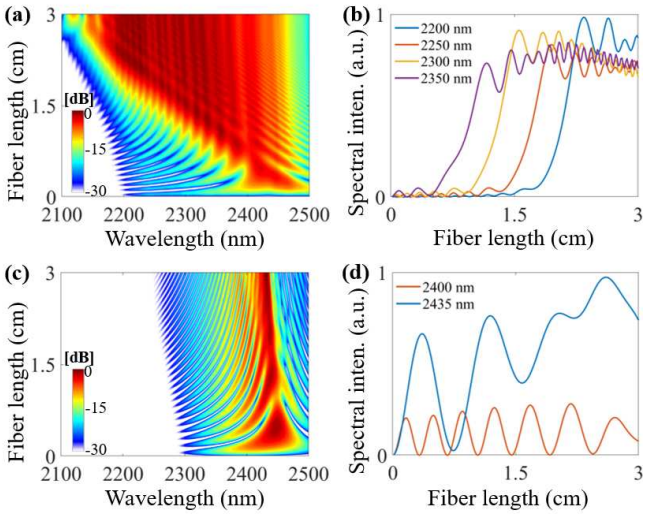

FIG. 3. Numerical simulation of mid-IR idler spectral evolution corresponding to the experiments for (a,b) a fiber with 4.2 μm to 3.6 μm core diameter taper and (c,d) an untapered fiber with 4.2 μm diameter.

To demonstrate AFWM, we conducted the experiment depicted in Fig. 2(a). Two pump beams were derived from a Yb^{3+}:YAG laser and its second harmonic (Pump A: 1030 nm wavelength, 3 ps duration, 110 nJ energy, and Pump B: 515 nm, 2 ps, 23 nJ). These were combined with a broadband and relatively weak chirped 1-ps near-infrared signal pulse derived from an optical parametric amplifier (Signal: 700-740 nm spectral width, 37 fs if fully compressed, 1 nJ). The diameter of each beam was adjusted so a single achromatic objective lens could efficiently couple each beam to its fundamental mode in the PCF. Silica fiber with high air-fraction cladding (shown in Fig. 2(b)) was tapered by a redrawing process of simultaneous local heating with an oxy-butane flame and stretching [28, 29]. A roughly linearly tapered section with core diameter of 4.2 μm to 3.6 μm was cut from the fiber, covering $\Delta k_{\text{eff}} = 0$ conditions for a signal (idler) range of 700-723 nm (2180-2430 nm) (Fig. 2(c)). The small fiber core diameter and thus tight mode confinement produced a strong waveguide dispersion dependence on core diameter, allowing a significant longitudinal sweep $\Delta k_{\text{eff}}(z)$ through zero for each set of signal-idler pairs and fulfilling Eq. 2 at sufficiently high pump power. As we aimed to achieve AFWM while suppressing other possible FWM processes, we minimized the ratio $L_{ad}/L_{NL} = 1/\kappa$ by maximizing the pump power and minimizing the taper length to 3 cm (see Supplemental Material for further discussion). A CaF_2 lens was placed after the PCF to collect the mid-IR idler spectrum, followed by a Ge window (anti-reflection coated for 1.9-6 μm) to block the pumps and residual signal and an InGaAs spectrometer. These were alternatively replaced by a silica lens, bandpass filter (590-740 nm), and Si spectrometer when analyzing the signal spectrum.

Observations of the idler generation verified the presence of AFWM frequency conversion in the tapered fiber vs. standard conversion in an untapered fiber (Fig. 2(d)). When the three input beams were coupled predominantly into the fundamental modes of the larger (4.2-μm diameter) end of the tapered PCF and synchronized in time, idler generation over the full 2180-2430 nm range was observed. In comparison, with the fiber replaced by an untapered 4.2-μm diameter PCF of the same length, a narrow idler band was observed at 2430 nm.

These measurements were tested against numerical solutions of a generalized nonlinear Schrdinger equation model [16, 30] of the four broadband fields in our experiment, assuming a linear PCF taper (Fig. 3). These indicate a clear difference between the evolution dynamics of the idler in the tapered (a,b) and the untapered (c,d) fibers. Conversion occurs sequentially by wavelength in the tapered case (a), occurring first for longer wavelengths, as expected. Frequency line-outs (b) show the characteristic form of adiabatic passage shown in Fig. 1(f): a rapid photon population inversion where the system passes through $\Delta k_{\text{eff}} = 0$, followed by an attenuating and accelerating oscillation as the wave momen-

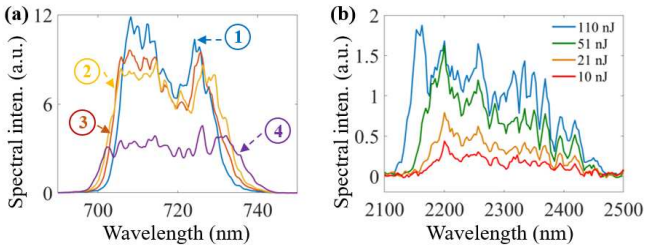

FIG. 4. (a) Measured signal spectra under various input beam conditions: ① signal only; ② signal + Pump B; ③ signal + Pump A; ④ signal + both pumps. (b) Measured idler spectra for varying Pump A (1030 nm) energy.

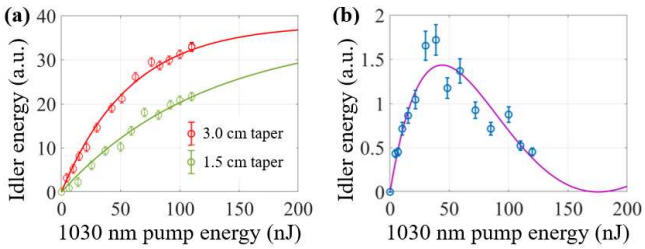

FIG. 5. Integrated idler energy from the tapered (a) and untapered (b) fibers, with respective fits to LZ and Rabi-oscillation models of pump energy dependence.

tum becomes mismatched ($\Delta k_{\rm eff} \neq 0$) and coupling is adiabatically reduced. The simulated and experimental output idler spectra display a close correspondence (Fig. 2(d)). The fast ripple in the simulated idler spectrum is due to the varying phase of the decaying Rabi oscillation by frequency and can be only partially resolved in the experimental spectrum due to limited resolution. In contrast, the untapered fiber (Fig. 3(c,d)) produces an idler evolution exhibiting Rabi-like conversion-back-conversion cycles as in Fig. 1(c), but with deviations due to an XPM-induced frequency blue-shift. Moreover, as expected, its conversion bandwidth narrows with length due to the inhomogeneous oscillation period of the ensemble of photon frequencies (i.e., the idler frequencies having different fixed $\Delta k_{\rm eff}$). Again, the simulated and measured output spectra closely match (Fig. 2(d)). The roughly 25-times larger bandwidth of the tapered fiber (representing a dramatic practical advantage) confirms the feature of AFWM to allow efficient population inversion in the presence of both significant ensemble inhomogeneity and parasitic XPM, as discussed below.

The blue shift noticeable in both fibers is attributed to the joint occurrence of XPM and temporal walk-off between pulses. Evidence is found in the experimental spectra in Fig. 4. As SPM and XPM are automatically wave-vector-matched processes, these cubic nonlinear effects are expected to accompany FWM frequency conversion. At signal and idler wavelengths, XPM driven by the brighter pump waves are the dominant effect. Fig. 4(a) shows the measured depletion of the near-IR signal spectrum accompanying generation of the idler. When either pump wave is present but not both (traces ②, ③), FWM frequency conversion does not occur, but mild spectral broadening of the signal is observed, a signature of XPM occurring due to nonlinear polarization terms $P_{\rm Sig} \propto \chi^{(3)}(|E_{\rm A}|^2 + |E_{\rm B}|^2)E_{\rm Sig}$. With both pumps present (trace ④), the signal is significantly and uniformly depleted across its entire bandwidth by FWM with a greater degree of XPM-induced broadening. In the idler spectrum (Fig. 4(b)), XPM-induced spectral broadening increases as Pump A pulse energy is increased (while keeping Pump B energy fixed at 23 nJ). This is due to nonlinear polarization term $P_{\rm Idl} \propto \chi^{(3)}|E_{\rm A}|^2 E_{\rm Idl}$ along with a shift to shorter wavelengths, a consequence of XPM in the presence of an advance at a rate of 0.11 ps/mm of the 1030-nm pump pulse relative to the idler pulse during propagation due to their group-velocity mismatch. The resulting greater overlap with the 1030-nm pulse trailing edge, where blue spectral shifts are generated, compared to the leading edge, where red spectral shifts are generated, results in an overall blue shift.

We expected AFWM efficiency as high as 72%, the fraction of input signal energy within the PCFs designed conversion bandwidth (700-723 nm). The observed fractional signal energy depletion (evaluated by comparative integration of purple and blue curves in Fig. 4(a)), however, was 50%, indicating a ∼70% population inversion, limited by damage to the fiber at higher pump powers. Fig. 5(a) shows the integrated mid-IR idler energy for varying Pump A pulse energy with Pump B pulse energy fixed at 23 nJ for tapered fibers of 3.0-cm (red) and 1.5-cm (green) length, each having the same 4.2 μm to 3.6 μm core diameter taper and with all other experimental parameters kept fixed. These data fit well to the LZ form $y = a(1 - \exp(-b \cdot x))$ and match the form of Fig. 1(f), clearly indicating adiabatic conversion. As expected, a higher conversion rate (greater adiabaticity) is observed for the longer fiber due to its having half the taper rate and thus half the $|\Delta \dot{k}_{\rm eff}|$ of the shorter fiber. In fact, we find $b_{\rm 3cm}/b_{\rm 1.5cm} = 2.1 \pm 0.8$, close to the ratio 2 as expected from Eq. 3. $a_{\rm 3cm} = 38.0(\pm 3.1)$ a.u. and $a_{\rm 1.5cm} = 36.3(\pm 8.9)$ a.u. also closely match, as expected, as the total energy coupled into the fibers should not vary between experiments. (For corresponding signal energy curves, see Supplemental Material.) In contrast, Fig. 5(b) shows the same data for a 3-cm untapered fiber, which cannot be fit to an exponentially saturating LZ efficiency function due to the apparent back-conversion. Rather, the data fit well to the $y = a \cdot \sin^2(b \cdot x)$ dependence of a resonant Rabi oscillation, as seen in Fig. 1(c). Fig. 5(a) clearly indicates that a higher pump energy or longer taper should result in fuller conversion. While damage to the fiber at higher intensity and large

group-velocity walk-off between idler and pump pulses in longer fibers restricted this study, optimization to further expand the efficiency and bandwidth (and to cover other spectral ranges) might be carried out through appropriate design of the PCF structure and choice of material. For example, tight mode confinement in the chosen PCF resulted in some mode area mismatch that reduced the effective coupling strength and overall conversion efficiency. A wider fiber core as might be used for higher pulse energy applications could eliminate this factor.

Applied to other fiber or waveguide platforms, broadband and efficient RAP by FWM frequency conversion could solve a number of current problems in quantum optics and laser physics fields. BS FWM has already been used to demonstrate frequency-domain Hong-Ou-Mandel interference with ultralow $g^{(2)}$ [7]. An adiabatic BS FWM process could be used for precise and uniform control of the photon splitting ratio over greatly widened bandwidths and potentially used in low-loss all-fiber or on-chip platforms. As shown, the adiabatic phase matching approach also allows a broad conversion bandwidth for spectral regions separated by multiple octaves, and overcomes the traditional restriction of working at wavelength ranges with low dispersion for broadband wave mixing in either BS FWM or degenerate-pumped FWM applications, such as close to a zero-dispersion-wavelength [4, 7, 25]. For high-intensity, ultrashort pulse applications, the weak dispersion of gas phase media in hollow core fibers could allow multiple octaves of conversion bandwidth while accommodating multi-mJ pulse energies. As predicted [30], the combination of gas medium and micro-structured waveguide as available in anti-resonant and photonic bandgap fiber might be used to translate the frequency of energetic few-cycle pulses to mid-IR frequencies desirable for driving strong-field processes, and is a platform also relevant to the generation of vacuum-UV light [31]. Pressure or temperature gradients might alternatively be used to sweep Δk_{eff} in these platforms [16, 30, 32, 33]. Looking ahead, study of the pump depletion regime of adiabatic frequency conversion - which was found to retain some of the character of RAP dynamics in TWM [34, 35] - may be valuable for AFWM applications where pump intensity is limited or efficient pump conversion is desired. More generally, through the Hermitian and unitary operation of RAP combined with BS FWM, AFWM enables precise control of the two-dimensional Hilbert space of light fields coupled through a nonlinear polarizability present in all media while solving the limited momentum-matching acceptance bandwidth problem, and thus can be expected to expand parametric frequency conversion to a wide set of future uses, both fundamental and applied.

Support was initially provided by the Air Force Office of Scientific Research (FA9550-15-1-0356) and United States-Israel Binational Science Foundation (BSF) (2014360), and later by the Office of Naval Research (N00014-19-1-2592). D.H. was supported by the Dept. of Defense National Defense Science Engineering Graduate Fellowship (NDSEG) Program. The authors thank Logan Wright for helpful discussions, Yuxing Tang, Michael Buttolph, and Walter Fu for help cleaving fibers, and Jim Stone for supplying the fibers. The data underlying the results in this paper are available at [36].

* moses@cornell.edu

[1] P. Kumar, Opt. Lett. **15**, 1476 (1990).
[2] C. J. McKinstrie, J. D. Harvey, S. Radic, and M. G. Raymer, Opt. Express **13**, 9131 (2005).
[3] T. Kobayashi, R. Ikuta, S. Yasui, S. Miki, T. Yamashita, H. Terai, T. Yamamoto, M. Koashi, and N. Imoto, Nat. Photonics **10**, 441 (2016).
[4] S. Clemmen, A. Farsi, S. Ramelow, and A. L. Gaeta, Phys. Rev. Lett. **117**, 223601 (2016).
[5] A. Karnieli and A. Arie, Optica **5**, 1297 (2018).
[6] H. J. McGuinness, M. G. Raymer, C. J. McKinstrie, and S. Radic, Phys. Rev. Lett. **105**, 093604 (2010).
[7] C. Joshi, A. Farsi, S. Clemmen, S. Ramelow, and A. L. Gaeta, Nat. Commun. **9**, 847 (2018).
[8] L. D. Landau, Phys. Sov. Union **2**, 46 (1932).
[9] C. Zener, Proc. R. Soc. of London **137**, 696 (1932).
[10] F. Bloch, Phys. Rev **70**, 460 (1946).
[11] M. M. Loy, Phys. Rev. Lett. **32**, 814 (1974).
[12] H. Suchowski, D. Oron, A. Arie, and Y. Silberberg, Phys. Rev. A **78**, 063821 (2008).
[13] J. Moses, H. Suchowski, and F. X. Kärtner, Opt. Lett. **37**, 1589 (2012).
[14] H. Suchowski, P. R. Krogen, S.-W. Huang, F. X. Kärtner, and J. Moses, Opt. Express **21**, 28892 (2013).
[15] P. Krogen, H. Suchowski, H. Liang, N. Flemens, K.-H. Hong, F. X. Kärtner, and J. Moses, Nat. Photonics **11**, 222 (2017).
[16] E. Bahar, X. Ding, A. Dahan, H. Suchowski, and J. Moses, Opt. Express **26**, 25582 (2018).
[17] P. B. Corkum and F. Krausz, Nat. Phys. **3**, 381 (2007).
[18] F. Krausz and M. Ivanov, Rev. Mod. Phys. **81**, 163 (2009).
[19] P. Colosimo, G. Doumy, C. Blaga, J. Wheeler, C. Hauri, F. Catoire, J. Tate, R. Chirla, A. March, G. Paulus, *et al.*, Nat. Phys. **4**, 386 (2008).
[20] L. Chipperfield, J. Robinson, J. Tisch, and J. Marangos, Phys. Rev. Lett. **102**, 063003 (2009).
[21] C. I. Blaga, J. Xu, A. D. DiChiara, E. Sistrunk, K. Zhang, P. Agostini, T. A. Miller, L. F. DiMauro, and C. Lin, Nature **483**, 194 (2012).
[22] Y. S. You, M. Wu, Y. Yin, A. Chew, X. Ren, S. Gholam-Mirzaei, D. A. Browne, M. Chini, Z. Chang, K. J. Schafer, *et al.*, Opt. Lett. **42**, 1816 (2017).
[23] D. Polli, P. Altoè, O. Weingart, K. M. Spillane, C. Manzoni, D. Brida, G. Tomasello, G. Orlandi, P. Kukura, R. A. Mathies, *et al.*, Nature **467**, 440 (2010).
[24] L. J. Wong, K.-H. Hong, S. Carbajo, A. Fallahi, P. Piot, M. Soljačić, J. D. Joannopoulos, F. X. Kärtner, and I. Kaminer, Sci. Rep. **7**, 11159 (2017).
[25] J. B. Christensen, J. G. Koefoed, B. A. Bell, C. J. McKinstrie, and K. Rottwitt, Opt. Express **26**, 17145 (2018).

[26] A. E. Willner, S. Khaleghi, M. R. Chitgarha, and O. F. Yilmaz, J. Light. Technol. **32**, 660 (2013).
[27] J. E. Midwinter, Appl. Phys. Lett. **12**, 68 (1968).
[28] T. A. Birks and Y. W. Li, J. Light. Technol. **10**, 432 (1992).
[29] W. J. Wadsworth, A. Witkowska, S. G. Leon-Saval, and T. A. Birks, Opt. Express **13**, 6541 (2005).
[30] X. Ding, M. S. Habib, R. Amezcua-Correa, and J. Moses, Opt. Lett. **44**, 1084 (2019).
[31] P. S. J. Russell, P. Hölzer, W. Chang, A. Abdolvand, and J. Travers, Nat. Photonics **8**, 278 (2014).
[32] A. Markov, A. Mazhorova, H. Breitenborn, A. Bruhacs, M. Clerici, D. Modotto, O. Jedrkiewicz, P. di Trapani, A. Major, F. Vidal, and R. Morandotti, Opt. Express **26**, 4448 (2018).
[33] E. Rozenberg and A. Arie, Opt. Lett. **44**, 3358 (2019).
[34] O. Yaakobi, M. Clerici, L. Caspani, F. Vidal, and R. Morandotti, J. Opt. Soc. Am. B **30**, 1637 (2013).
[35] G. Porat and A. Arie, J. Opt. Soc. Am. B **30**, 1342 (2013).
[36] Data Repository, https://doi.org/10.15125/BATH-placeholder.